공학석사학위논문

공기 차압을 이용한 공기열원 열펌프의 제상시기 탐지방법에 대한 연구

Study on the Detection Method of Defrosting Start Time by Measuring Static Pressure Difference in Air Source Heat Pump System

2018 년 8 월

서울대학교 대학원

기계항공공학부

박 건 우

Abstract

Study on the Detection Method of Defrosting Start Time by Measuring Static Pressure Difference in Air source Heat Pump System

Keon Woo Park
Mechanical and Aerospace Engineering
The Graduate School
Seoul National University

This study shows the feasibility and effectiveness of the detection method for determining the defrosting start time by measuring the air static pressure differences between the atmospheric pressure and the pressure measured before the outdoor unit fan in air source heat pump system (ASHP).

Generally, the frosting occurs under cold and humid environmental air condition, which means outdoor air temperature around the heat exchanger is lower than both dew point temperature of air and freezing temperature of water.

As the frost accumulation increases, the air pressure differences occur

between the atmospheric pressure and the pressure measured inside the outdoor unit because of becoming narrow the area of airflows. It is possible to predict the frost accumulation of the heat pump evaporator indirectly measuring these changes of the pressure differences.

The pressure of the air is consist of the static pressure and dynamic pressure. The static pressure is used for obtaining the consistent and reliable data for the airflows. If the dynamic pressure is used, the experimental data will be influenced by the position of the differential pressure sensors and be possible of being blocked by the dust or moisture. On the contrary, if we use the static pressure, the negative pressure occurs at the position of measuring the pressure inside the outdoor unit. When the outdoor fan operates, the pressure inside the outdoor unit becomes lower than the external pressure and the negative pressure is generated. This shows that the possibility of going the dust or moisture inside sensors is minimized and the static pressure is less influenced by the change of the air velocity unlike the dynamic pressure.

The pressure measurement position inside the outdoor unit is an important factor in this study. The heat exchanger is generally divided into three parts such as high, middle and low. As the pressure is measured at a position close to the fan, the value of the static pressure increases. On the contrary, it gets the lower static pressure value being farther away from the fan.

As the frost accumulation increases, the air pressure differences between the atmospheric pressure and the pressure inside the outdoor unit also increases.

It shows that the position of measuring the pressure is getting lower, the pressure differences become bigger.

Measuring the pressure at the same height, the distance between the measuring point and the heat exchanger is an important factor to consider.

The pressure is measured at five locations: center, front, rear, right, and left to find the optimal position at the same height. The distance between each sensor is 8 cm and the right position is about 3 cm away from the outdoor heat exchanger.

The differential pressure value increases as the pressure measurement position is closer to the heat exchanger due to the influence of the airflows.

The performance of various operating conditions such as pressure measurement position, outdoor air temperature, relative humidity and compressor speed is tested to identify the relation of pressure drop with heating capacity of the system. The pressure difference control method is suggested by providing an appropriate threshold value and comparing with the result with other estimation methods.

As a result, the suggested method is more reliable than conventional time control method for deciding the defrosting start time.

Conclusively, the defrosting start time can be controlled by measuring the air static pressure difference between the atmospheric pressure and the pressure measured before the outdoor unit fan in air source heat pump system.

Keywords: Air source heat pump, Defrosting cycle, Frost deposition, Static pressure difference

Student Identification Number: 2016-27922

Contents

Abstract i

Contents v

List of Tables viii

List of Figures ix

Nomenclatures xi

Chapter 1. Introduction 1

1.1 Background of the study 1

1.2 Literature survey 7

1.2.1 Various methods to determine the defrosting start time 8

1.2.2 Application of the differential pressure 11

1.3 Objectives and scopes 12

Chapter 2. Experimental setup and procedures 14

2.1 Introduction 14

2.2 Experimental procedures and conditions 21

2.3 Data reduction and uncertainty analysis 22

2.4 Static pressure 25

2.5 Position of measuring the pressure 25

Chapter 3. CFD analysis of the pressure distribution inside of the outdoor unit 27
3.1 Introduction 27
3.2 Description of CFD Model and boundary conditions 28
3.3 CFD analysis result 31
3.3.1 Pressure distribution in no frosting condition 31
3.3.2 Pressure distribution in frosting condition 33
3.4 Summary 36

Chapter 4. Experimental results by measuring differential pressure 37
4.1 Introduction 37
4.2 Optimal position of sensing the static pressure 39
4.2.1 Optimal position at the same height 39
4.2.2 Optimal position at the different height 45
4.3 Pressure differences under various conditions 47
4.3.1 Various dry-bulb temperature conditions 47
4.3.2 Various relative humidity conditions 50
4.3.3 Various compressor speed conditions 52
4.3.4 Various fan speed conditions 54
4.4 Summary 56

Chapter 5. Conclusion 59

References 60
Abstract (Korean) 63

List of Tables

Table 2.1 Specification of the heat pump system.....17

Table 2.2 Experimental conditions.....23

Table 2.3 Uncertainty analysis at rating condition.....24

Table 4.1 Comparison of the defrost cycle start time according to the different determination method.....58

List of Figures

Figure 1.1 Gobal Air Conditioning Market 2

Figure 1.2 Frosting accumulation pictures of the heat exchanger 4

Figure 1.3 P-h diagram with performance drop.....5

Figure 1.4 Various defrosting start time determination methods.....10

Figure 2.1 The schematic of experimental set up 15

Figure 2.2 The psychometric chamber (10 RT).....16

Figure 2.3 The simple diagram of differential pressure measurement 19

Figure 2.4 Control panel of LABVIEW prog Real time estimation of variables in LABVIEW program.....20

Figure 3.1 Geometry of the outdoor unit 30

Figure 3.2 CFD analysis results in no frosting 34

Figure 3.3 CFD analysis results in frosting 35

Figure 4.1 Pressure differences and heating capacity in a high position 42

Figure 4.2 Pressure differences and heating capacity in a middle position ..43

Figure 4.3 Pressure differences and heating capacity in a low position 44

Figure 4.4 Pressure differences and heating capacity according to measuring position 46

Figure 4.5 Heating capacity ration and pressure difference under various dry-bulb temperature 49

Figure 4.6 Heating capacity ratio and pressure differences under various relative humidity 51

Figure 4.7 Heating capacity ratio and pressure differences under various compressor speed 53
Figure 4.8 Heating capacity ratio and pressure differences under various fan speed.....55

Nomenclatures

A	area (m^2)
COP	coefficient of performance
DSC	degree of subcool (K)
DSH	degree of superheat (K)
d	diameter (mm)
EEV	electronic expansion valve
P	static pressure (Pa)
q	specific capacity (kJ/kg)
Q	heating capacity (kW)
RH	relative humidity (%)
i	enthalpy (kJ/kg)
T	temperature (K)
T_{dc}	temperature under differential pressure control (˚C)
T_{std}	temperature under standard control (˚C)
T_{tc}	temperature under time control (˚C)
$\dot{V}$	volume flow rate (m^3/s)
v	velocity (m/s)
W	Compressor work (kW)

Subscript

Cond	condenser
comp	compressor
Eva	evaporator
in	inlet
liq	liquid
out	outlet
ref	refrigerant side
vap	vapor

Chapter 1. Introduction

1.1 Background of the study

The environmental issues such as climate change and global warming are emerging as the consumption of fossil fuel is increasing. To reduce the consumption of fossil fuel causing the environmental pollution is necessary to use energy efficiently. For this reason, the air source heat pump (ASHP) has been received much attention in many years due to its energy saving, high efficiency and environmental protection. The air source heat pump system has been used for many years with easy installation and economical operation costs. Fig. 1.1 shows the growth of the global air conditioning market from 2012 to 2017. The global sales volume of air conditioners will increase by about 30% from 120 million units in 2012 to 160 million units by 2017.

Despite the constant growth of air conditioners, there are noticeable problems awaiting solution such as frosting accumulation on the heat exchanger and mal defrosting. The frosting occurs under cold and humid environmental air condition, which means outdoor air temperature around the heat exchanger is lower than both dew point temperature of air and freezing temperature of water. If the frosting occurs and accumulates on the outdoor heat exchanger like Fig. 1.2, these negative factors lead to the heating capacity and efficiency decrease and undesired shutdown happens.

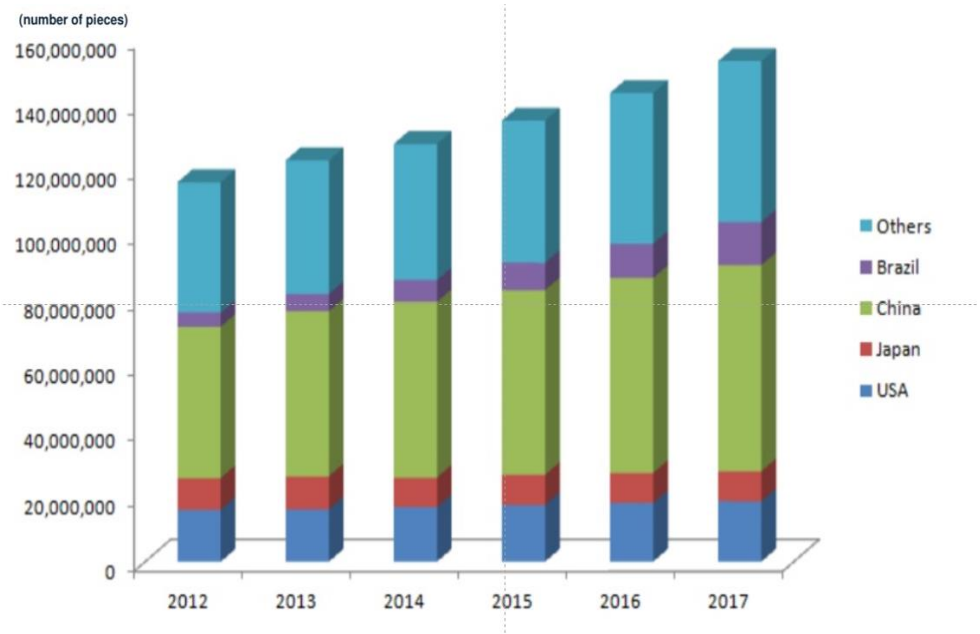

Fig. 1.1 Global Air Conditioning Market (2012-2017)

(BSRIA, 2014)

There are two reasons why the deposited frost deteriorate heating capacity. First, it blocks airflow and causes increase of air pressure drop and decrease of airflow rate. Second, Breque and Nemer (2017) showed that the frost layer on the fin area becomes an additional thermal resistance at the evaporator.

These unfavorable factors lead to decrease the heat transfer capacity of the evaporator and finally the heating capacity of air source heat pump system as shown Fig. 1.3. Wang et al. (2011) conducted field experiment and showed that the heating capacity of ASHP will decrease 29%~57% when the outdoor heat exchanger is covered by the frost layer. Song et al. (2018) showed that frosting duration accounts more than 80% of operation time in a frosting-defrosting cycle, and thus frost retarding measure exploration play important roles in optimization of ASHP units

To remove the accumulated frost, it is necessary that defrosting cycle be activated at proper intervals. The defrosting cycle is generally similar to a cooling operation and is the most commonly used method of defrosting. The refrigerant of high temperature and high pressure discharged from the compressor is not sending to the indoor unit but sending to the outdoor unit heat exchanger by using the four-way valve to dissolve the frosting. However, this method requires the interruption of heating mode during defrosting cycle and interval time to reheat the cooled heat exchanger of the outdoor unit after melting the frost. It is also essential that defrosting control must be implemented on demand whatever kind of method is used.

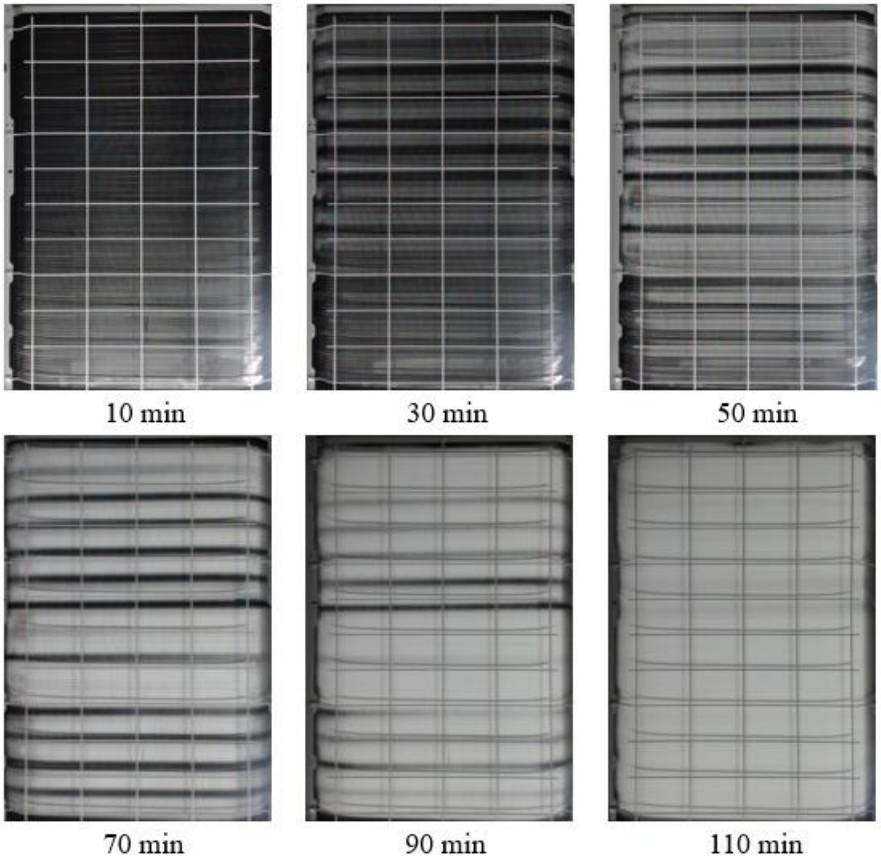

Fig. 1.2 Frosting accumulation pictures of the heat exchanger

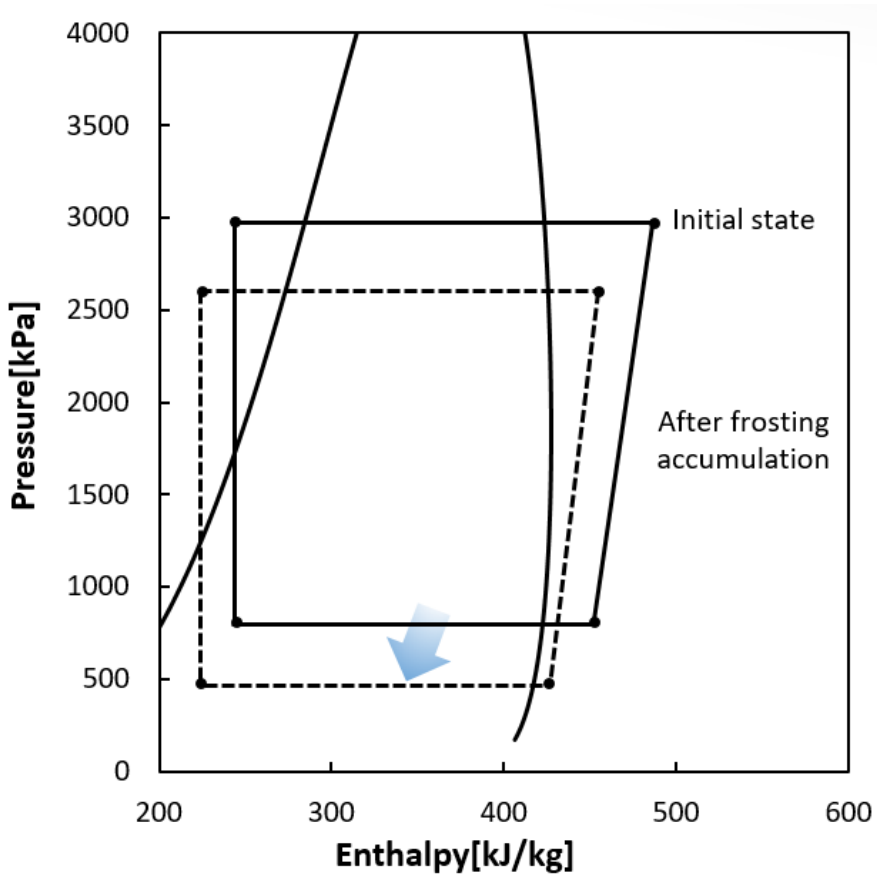

Fig. 1.3 P-h diagram with performance drop

It is difficult to predict the exact defrosting start time. Because the field condition of frosting changes every moment depending on the air temperature and humidity around the outdoor unit, and the heating load of indoor space. In some cases, unnecessary defrosting is performed in spite of monitoring many parameters such as air temperature, air relative humidity, fin temperature, running time for heating cycle etc. This phenomenon is called 'mal defrosting'. According to the study of Wang et al. (2011) mal defrosting could be inevitable and random in the practical application.

Wang et al. (2011) classified this 'mal-defrosting' control into two types. One is that early defrosting cycle is performed under no-frosted or little-frosted conditions, and the other is that defrosting cycle is not executed even after the frosting has been considerably progressed. Thus, it is necessary to properly start the defrosting cycle to gain adequate heating capacity. It is observed that the mal defrosting control reduced COP and heating capacity to 40.4% and 43.4% respectively.

Some control methods are heavily dependent to the system specification (artificial neural network control, and frost map control), while some other methods require high cost (Optical control) or complicated scheme to deal with unexpected system operations (Flow instability sensing control, and DSH sensing control). Thus, it is necessary to develop a defrosting control method with high simplicity, adequate universality, and low price.

Defrosting control with air differential pressure is a suitable solution to the necessities.

1.2 Literature survey

1.2.1 Various methods to determine the defrosting start time

To remove the accumulated frost, it is necessary that defrosting cycle be activated at proper intervals. To do this, it is important to determine whether it is proper time to start defrost cycle operation. There have been several studies that suggest determination criteria of defrost cycle operation as shown Fig. 1.4.

Zhu et al. (2015) developed a frosting map to guide defrosting control. Kim et al. (2015) and Jiang et al. (2013) proposed novel defrosting control method based on effective mass flow fraction of air passing outdoor unit. Mengjie et al. (2018) reviewed that several researchers also suggested studies for the defrosting control using photo-coupler.

Basically, Zhu et al. (2015) showed that time control (T-C) method and temperature-time control (T-T-C) method are the most widely used defrosting control method. The commercial products uses this time control method due to its low cost and simple control. While time control is the simplest method using only operation time as a basis for the determination, it is not suitable under various operating conditions. Because, time control method (T-C) do not consider outside air temperature, humidity, refrigerant pressure, surface temperature of heat exchanger. Even for the time-temperature control (T-T-C) developed from time control (T-C), temperature and time data are not enough to determine the defrost cycle start time

properly under various operating conditions.

According to Baxter et al. (1985), approximately 27% of defrosting cycle in a test heat pump with time-temperature control (T-T-C) was not necessary. Ge et al. (2016) reported that wasted work due to the unnecessary defrosting is reduced by 62.2%. It is because not only the time and temperature, but also other information such as humidity and heat pump operation condition has important role on frost accumulation. Time-temperature control (T-T-C) is kind of an indirect method that has also possibility of mal defrosting control. Some researchers suggested to adopt photo-coupler sensor for the defrost control.

Defrost cycle start time is determined by measuring regional frost thickness using photo-coupler sensor. Byun et al. (2006) installed several sensors at the heat exchanger, and proposed optimum defrost cycle start point that maximize the heat pump performance. Wang et al. (2013) repeated heat pump operation with frost-defrost cycle, which is determined by photo-coupler sensor. The study reported that heat pump operation with suggested defrost control can improve heating efficiency up to 92.6% compared to the operation with conventional time control (T-T).

In spite of the advantages of photo-coupler sensor, it is hard to be applied to commercial products. Since the sensor only can measure regional point of the heat exchanger, a number of sensor is needed to reliably determine proper defrost cycle start time.

In addition, the current photo-coupler sensor is expensive and has short lifespan,

which makes it hard to be used commercially. The main defrosting control methods currently in use can be summarized as follows. Time control (T-C) and time temperature control (T-T-C) have low accuracy under various operating conditions and have possibility of mal-defrosting. One of the direct measurement method is photo-coupler control that has good accuracy but has high price and low durability.

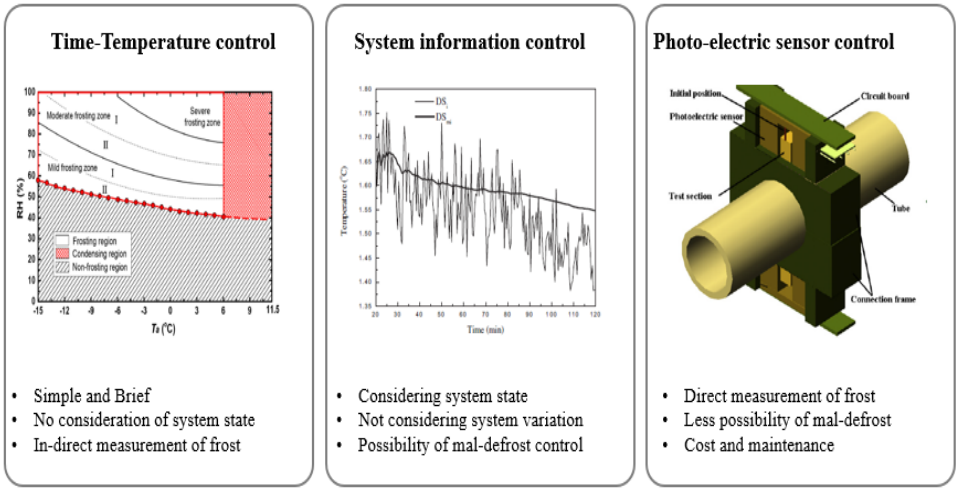

Fig. 1.4 Various defrosting start time determination methods

1.2.2 Application of the differential pressure

Kim et al. (2015) showed that differential pressure control measures the flow resistance between the air side inlet and outlet to determine the presence of a frost layer. This technique can effectively determine defrost start time, but is expensive and a short lifespan. However, recent developments in technology have led to a decrease in the price of differential pressure sensors used for differential pressure measurement and increased durability, which can be used in a variety of ways to determine the defrosting start time compared to other previous methods. In the past pressure measurement experiment, the pressure according to the frosting was measured by installing a differential pressure sensor before and after the compact heat exchanger. In this study, the differential pressure sensor is applied to the commercial ASHP, which is the most commonly used. Feasibility and effectiveness of the suggested defrost control is investigated from the experiment with commercial heat pump system of 26 kW heating capacity. Since the deposited frost causes the increase of the pressure drop, air pressure difference between back end of heat exchanger and ambient air increases as frost is accumulated at the heat exchanger.

The pressure of the air is consist of the static pressure and dynamic pressure. The static pressure is used for obtaining the consistent and reliable data for the airflow. If the dynamic pressure is used, the experimental data will be influenced by the position of the differential pressure sensors and be possible of being blocked by the

dust or moisture. On the contrary, if we use the static pressure, the negative pressure occurs at the position of measuring the pressure inside the outdoor unit. When the outdoor fan operates, the pressure inside the outdoor unit becomes lower than the external pressure and the negative pressure is generated. This shows that the possibility of going the dust or moisture inside sensors is minimized and the static pressure is less influenced by the change of the air velocity unlike the dynamic pressure.

The static pressure difference sensor is established inside of the outdoor unit. Experiment is carried out under several outdoor air conditions and system operation conditions to verify the suggested defrost control method. According to the experimental results, it is verified that the suggested method can achieve high reliability for the determination of defrost cycle start.

1.3 Objectives and scopes

Differential pressure value differs depending on the measurement position of differential pressure sensor. It is an important factor to find the optimal position of the pressure measurement inside the outdoor unit in this study.

The objective of this study is to find the methods to determine the optimal defrosting start time in air source heat pump. CFD (Computer Fluid Dynamics) analysis and experiments are performed to find out the optimal position where the

change of pressure difference occurs mostly high and to investigate the characteristics of differential pressure under various operating conditions.

In chapter 2, experimental set up, procedures and the optimal pressure measurement height and distance from the heat exchanger are proposed. The heat exchanger is generally divided into three parts such as high, middle and low. Measuring the pressure at the same height, the pressure is measured at five locations: center, front, rear, right, and left to find the optimal position at the same height.

In chapter 3, the pressure variation due to frosting using CFD simulation of the air source heat pump system is introduced. By interpreting the change in the internal pressure of the outdoor unit caused by the frosting, the optimal differential pressure measurement position for the differential pressure test is predicted.

In chapter 4, the experiments are conducted under various operating conditions after applying for optimal pressure measurement position. The method for applying pressure difference to find the best defrosting start time efficiently is analyzed and suggested.

In the last chapter, a brief summary of the study and conclusion are given.

Chapter 2. Experimental setup and procedures

2.1 Introduction

Fig. 2.1 shows the schematic of the experimental set up. A split-type ASHP system is established for the experiment, and it has nominal 26 kW heating capacity. Two indoor units are used to match the capacity of the outdoor unit and indoor units. It also is equipped with a speed-controllable compressor, electronic expansion valve, and an accumulator. It is installed in two psychometric chambers as shown Fig. 2.2 to control the indoor and outdoor air conditions. The outdoor heat exchanger is a rounded tube and louvered fin heat exchanger. The tube is made of copper, while the louvered fin is made of aluminum. It is located on the three sides of the outdoor unit. The specifications of the outdoor heat exchanger are listed in Table 2.1.

Inverter-driven compressor is used for refrigerant compression. It has scroll type cylinder and stroke volume is 62.1 cm^3. The Sizes of the indoor and outdoor chambers are 33 m^3 and 33 m^3 respectively. In the outdoor chamber, air temperature is measured using resistance temperature detectors (RTD) and air relative humidity is measured using capacitive humidity sensor.

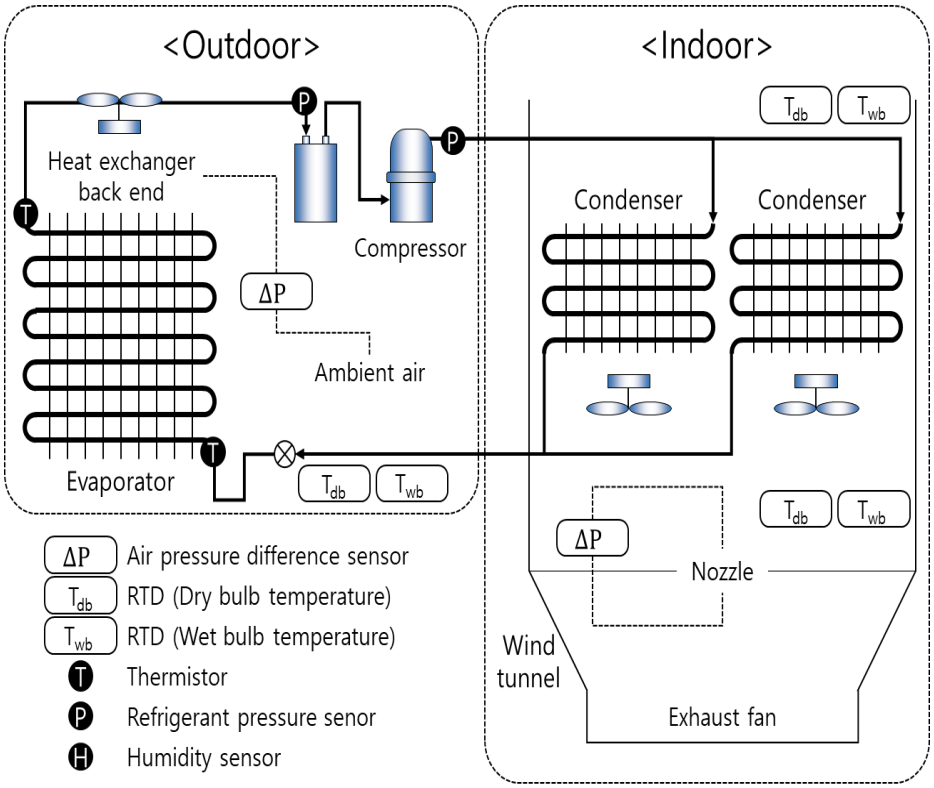

Fig. 2.1 The schematic of the experimental setup

Fig. 2.2 The psychometric chamber (10 RT)

Table 2.1 Specification of heat pump system

Part	Specifications
Compressor	Inverter-driven scroll compressor (Stroke volume : 62.1 cm^3)
Condenser side (2 indoor units)	Fin-tube heat exchangers (Fin pitch): 1.5 mm
Evaporator side (1 outdoor unit)	Fin-tube heat exchanger (Fin pitch): 1.3 mm
Expansion valve	Electronic expansion valve
Refrigerant	R410A, 9 kg
Outdoor Air fan	200 CMM @ 800 RPM

Differential pressure sensors (SDS) are installed to measure the pressure difference between inlet and outlet side of the outdoor evaporator. The location of the differential pressure sensor is presented in Fig. 2.3. As seen in the figure, one side of the differential pressure sensor is located inside of the evaporator, and the other side of the sensor is located outside of the evaporator. The optimum location of the differential sensor at the indoor side is determined from the CFD simulation, and detailed progress for the determination is presented in next chapter. In the indoor side, wind tunnel is installed to compute air side heating capacity.

Dry-bulb and wet-bulb temperatures are measured at the inlet and outlet side of the wind tunnel by RTD sensor to get enthalpy difference of the air flow passing the indoor condenser. Air density and enthalpy difference are calculated according to ASHRAE Handbook (2014). A nozzle is installed inside the wind tunnel to obtain air flow rate of the indoor side. Pressure difference between inlet and outlet side of the nozzle is measured, and it is used for air flow rate calculation following ANSI/AMCA 201. Total power consumption of the experimental set-up is also measured to get COP of the system using the LABVIEW program as shows in Fig. 2.4.

In the ASHP system, R410A is used for system refrigerant and optimum charge amount is determined to 9 kg from the preliminary experiment.

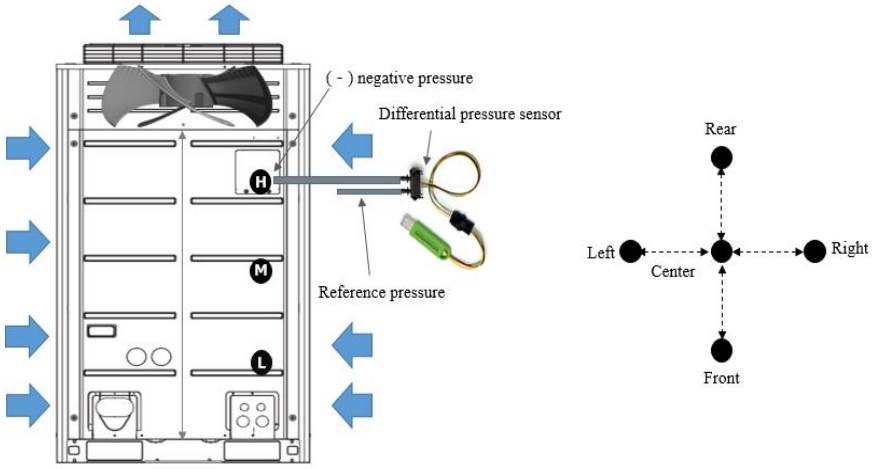

Fig. 2.3 The simple diagram of differential pressure measurement

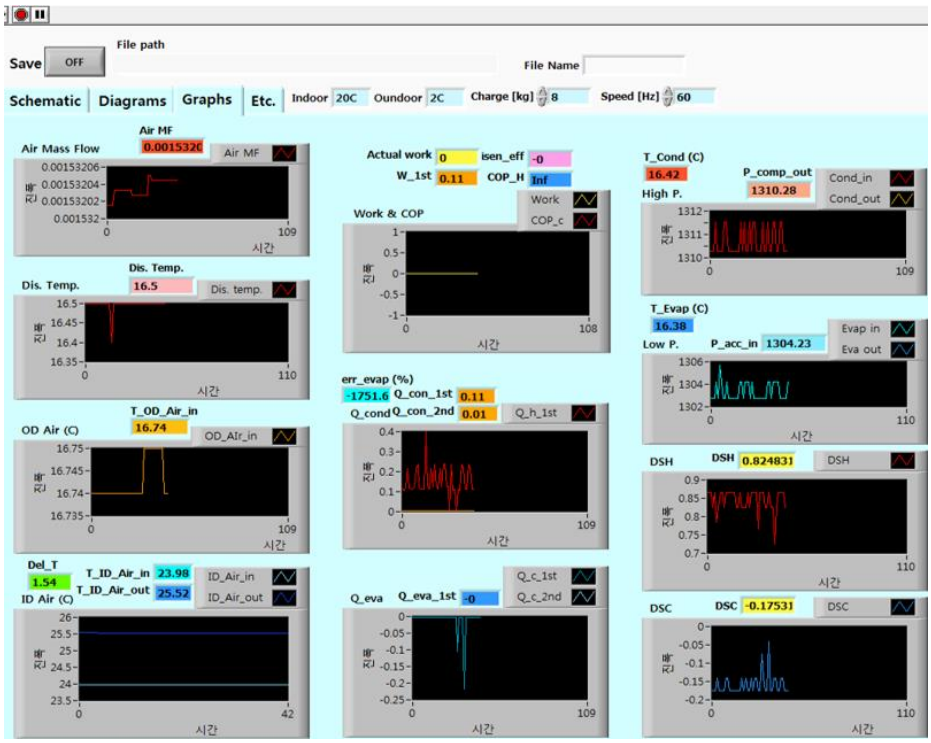

Fig. 2.4 Real time estimation of variables in LABVIEW program

The refrigerant temperature is measured in several points of the experimental set-up using T-type thermos couple. Refrigerant pressure is measured at the accumulator inlet and compressor outlet using pressure transducer. Mass flow rate of the refrigerant is obtained from Coriolis mass flow meter.

2.2 Experimental procedures and conditions

In this study, four control variables are chosen to include various frosting conditions; air temperature, air relative humidity, compressor speed and air fan speed. Experimental conditions are summarized in Table 2.2. Before the heat pump operation, psychometric chambers control the air temperature and humidity for enough time to set the air conditions. Especially for the indoor chamber, dry-bulb temperature and wet bulb temperature are set to 20 ℃ and 15 ℃ respectively. During the experiment, air temperature and relative humidity are maintained within ±0.5 ℃, and ±1%.

At the initial stage of the ASHP system start-up, compressor speed is increased gradually for 5 minutes to prevent the sudden undershoot of the refrigerant pressure. Then the compressor and air fan is running constantly at the designated speed until the frost is fully accumulated on the outdoor

evaporator.

EEV is controlled to maintain DSH to 5. Data acquisition is done from the compressor start-up, and to the operation stop. While operation, frontal area of the evaporator is visually recorded to observe the frosting progress.

Carstens et al. (2018) showed the measurement uncertainty in energy monitoring. The uncertainty analysis of the experiment is done as summarized in Table 2.3. Especially for the heating capacity and COP, uncertainty values are computed following ASHRAE Guideline 2. (2010).

2.3 Data reduction and uncertainty analysis

In this experiment, COP and heating capacity are obtained from Eqs. 3.1 and 3.2

$$Q_{air} = \rho_{air}\dot{V}_{air}(i_{air,out} - i_{air,in}) \tag{3.1}$$

$$COP = Q_{air}/W \tag{3.2}$$

The uncertainty analysis of the experiment is shown in Table 2.3. Among the uncertainty values, Maximum error for heating capacity and COP are 6.39% and 6.47% respectively on 95% confidence level. According to ASHRAE Guideline 2 (2010), the fractional uncertainty in the COP should not be greater than 10% and it is satisfied in this experiment.

Table 2.2 Experimental conditions

Case number	Dry-bulb temperature (℃)	Relative humidity (%)	Compressor speed (Hz)	Fan speed (RPM)
Case 1	-2	80	100	800
Case 2	-5	80	100	800
Case 3	1	80	100	800
Case 4	-2	70	100	800
Case 5	-2	90	100	800
Case 6	-2	80	75	800
Case 7	-2	80	100	960
Case 8	-2	80	100	640

Table 2.3 Uncertainty analysis at rating condition

Measurements	Fixed error	Random error	Total error
Pressure transducer (condenser side)	0.60%	0.39%	0.71%
Pressure transducer (evaporator side)	1.34%	0.27%	1.37%
Dry bulb air inlet temperature (RTD)	0.20 K	0.02 K	0.20 K
Wet bulb air inlet temperature (RTD)	0.19 K	0.06 K	0.20 K
Dry bulb air outlet temperature (RTD)	0.18 K	0.01 K	0.18 K
Wet bulb air outlet temperature (RTD)	0.18 K	0.03 K	0.18 K
Thermocouple (T-type)	0.50 K	1.52 K	1.60 K
Thermistor	0.70 K	0.32 K	0.76 K
Mass flow rate (refrigerant)	3.07%	0.77%	3.16%
Mass flow rate (air)	4.61%	0.50%	4.64%
Power consumption	0.20%	0.65%	0.68%
Heating capacity	6.28%	1.19%	6.39%
COP	6.28%	1.55%	6.47%

2.4 Static pressure

The pressure of the air is consist of the static pressure and dynamic pressure. The static pressure is used for obtaining the consistent and reliable data for the airflow. If the dynamic pressure is used, the experimental data will be influenced by the position of the differential pressure sensors and be possible of being blocked by the dust or moisture. On the contrary, if we use the static pressure, the negative pressure occurs at the position of measuring the pressure inside the outdoor unit. When the outdoor fan operates, the pressure inside the outdoor unit becomes lower than the external pressure and the negative pressure is generated. This shows that the possibility of going the dust or moisture inside sensors is minimized and the static pressure is less influenced by the change of the air velocity unlike the dynamic pressure.

2.5 Position of air static pressure measurement

It is an important factor to find the optimal position of the pressure measurement inside the outdoor unit in this study. The heat exchanger is generally divided into three parts such as high, middle and low as Fig. 2.5. The reason for installing the pressure sensor on the right side of the inside of the

outdoor unit is that there is no space for installing the sensor due to the parts such as 4way valve, accumulator, temperature sensors and refrigerant pressure sensors, pipes on the left and rear sides. As the pressure is measured at a position close to the fan, the value of the static pressure increases. On the contrary, it gets the lower static pressure value being farther away from the fan. As the frost accumulation increases, the air pressure differences between the atmospheric pressure and the pressure inside the outdoor unit also increases.

It shows that the position of measuring the pressure is getting lower, the pressure differences becomes bigger. Measuring the pressure at the same height, the distance between the measuring point and the heat exchanger is an important factor to consider. The pressure is measured at five locations: center, front, rear, right, and left to find the optimal position at the same height. The distance between each sensor is 8 cm and the right position is about 3 cm away from the outdoor heat exchanger. The differential pressure value increases as the pressure measurement position is closer to the heat exchanger due to the influence of the airflow.

Chapter 3. CFD analysis of the pressure distribution inside of the outdoor unit

3.1 Introduction

In this paper, Computer Fluid Dynamics (CFD) software is used for predicting the optimal pressure measurement position compared with traditional measurement method. CFD simulation technology is one of the most reliable methods, which could provide the accurate description of the air velocity (L.Shao and S.B.Riffat, 1995) and pressure distribution of inside the outdoor unit. The computations is performed using the commercial flow simulation software FLUENT. Varun Singh et al. (2011) showed that it is capable of accounting for air flow distribution and other complex flow patterns including recirculation zones within the heat exchanger, as well as, entrainment of exit flow into the heat exchanger, using both two-dimensional (2D) and three-dimensional (3D) CFD results. This results showed that the overall predicted heat load using 3D-CFD simulation results agrees within ±4% of the experimental data, without employing any multipliers on air side correlations.

As the frosting progresses, it is very hard work to measure the pressure in all areas. Because the pressure distribution inside the outdoor unit changes

diversely and there is no enough space for installing the many pressure sensors.

There are various parts in the outdoor unit such as 4way valve, accumulator, temperature sensors and refrigerant pressure sensors, pipes etc. Therefore, by comparing the pressure distribution analyzed through the CFD simulations with the pressure data measured through the actual experiment, the error value is known and the pressure value at the position where the actual sensor is not installed can be predicted.

3.2 Description of CFD Model and boundary conditions

In this paper, the pressure distribution inside of outdoor unit is analyzed and evaluated by CFD simulation method. Fig. 3.1 shows the modeling of the outdoor unit. The pressure distribution inside the outdoor unit due to the pressure drop in the heat exchanger is considered by referring to the performance data of the fan manufacturer. Since it is very difficult to interpret the CFD in the outdoor heat exchanger, the pressure difference between before and after the heat exchanger is applied to set the boundary condition when there is frosting and when there is no defrosting.

The model parameters are as follows:

(1) Outdoor unit dimensions (width x length x height):

930 mm x 1690 mm x 760 mm

(2) Fan volume and RPM: 200 CMM @ 800 RPM

(3) Fan diameter: 600 mm

(4) Fan type: Propeller type

(5) Fin pitch of fin tube heat exchanger: 1.3 mm

(6) Heat exchanger opening ratio (no frosting): 41.5% (experimental data)

(7) Heat exchanger opening ratio (frosting): 13% (experimental data)

(8) Outdoor air condition: Dry-bulb temperature at -2 ℃,

Relative humidity at 80%

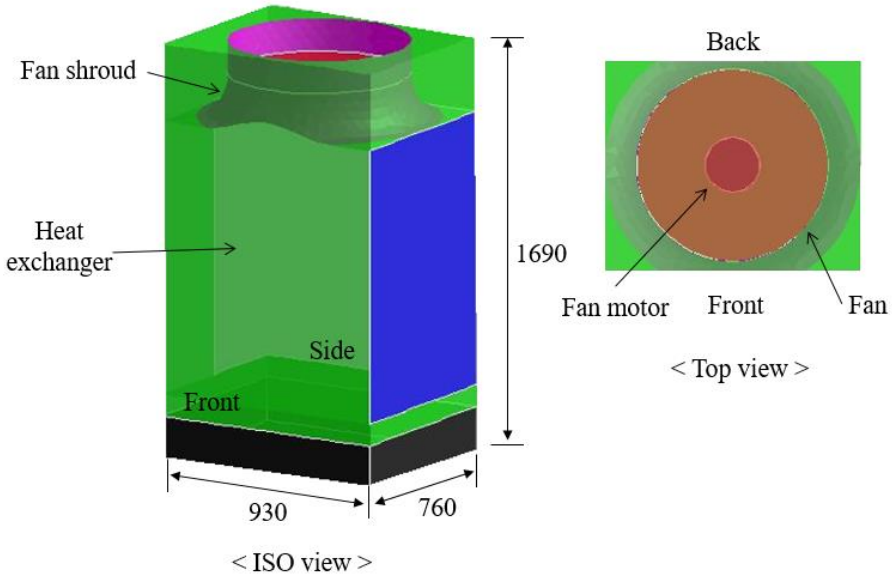

Fig. 3.1 Geometry of the outdoor unit

3.3 CFD analysis result

3.3.1 Pressure distribution in no frosting condition

Fig. 3.2 shows CFD analysis result of differential pressure distribution inside of outdoor unit in no frosting condition. The static pressure measured at a position close to the fan increases and it decreases for being away from the fan. The CFD analysis result shows that the negative pressure occurs at the position of measuring the pressure inside the outdoor unit. When the outdoor fan operates, the pressure inside of the outdoor unit becomes lower than the external pressure and the negative pressure is generated. The pressure measurement location is generally divided into three parts such as high, middle and low. The position of a high is 110 cm from the bottom of the outdoor unit. The middle is 80 cm from the bottom and low is 50 cm from the bottom.

The value of the static differential pressure is 107 Pa in a high position, 52 Pa in a middle position and 32 Pa in a low positon when there is no frosting.

The pressure difference between high position and middle position is 55 Pa, and the pressure difference between middle position and low position is 20 Pa. The distance between the every measurement positions is 30 cm, but the pressure difference is more than 2 times.

It can be seen that the differential pressure value becomes smaller as the

distance from the fan increases and the pressure value does not change in proportion to the distance difference of the measurement position.

The data below shows the high, middle and low pressure values in the top view with the same height. In the high position, the value of the static differential pressure at the center is 127 Pa and 62 Pa at the side. It can be seen that the pressure increases from the side to the center in the high position.

In the middle position, the value of the static differential pressure at the center is 52 Pa and 50 Pa at the side. The static pressure of side and center is almost the same unlike the result of the high position. This shows that the pressure inside of the outdoor unit is balanced both center and side position at the same height.

In the low position, the value of the static differential pressure at the center is 32 Pa and 32 Pa at the side. The static pressure of side and center is almost the same like the result of the middle position.

From these results, it can be seen that the static pressure increases from the low to high position in proportion to the pressure measurement height. On the other hand, the pressure increases from the side to the center in the high position, but the pressure values of the side and center are similar in the middle and low position with same height.

3.3.2 Pressure distribution in frosting condition

Fig. 3.3 shows differential pressure distribution inside of the outdoor unit in frosting condition. The frosting accumulation is almost maximum status and the blocking ratio is 87 %. Jhee et al. (2002) described that the blocking ratio was the total cross-sectional area of the air path that is blocked by the frosting layer and reported that defrosting should be initiated when the blocking ratio reaches the more than 80 %.

The value of the static differential pressure is 152 Pa in a high position, 132 Pa in a middle position and 127 Pa in a low positon. The pressure difference between the high position and middle position is 20 Pa and the pressure difference between middle position and low position is 15 Pa.

In previous test result in no frosting condition, the position of measuring the pressure is getting lower, the pressure differences becomes bigger.

On the contrary, the value of pressure differences tends to be similar to each other in frosting condition. This is because that the heat exchanger is almost blocked by the frost layer when the block ratio is over 80 % so that the air flow movement is reduced and the pressure inside of the outdoor unit is balanced both high and low position.

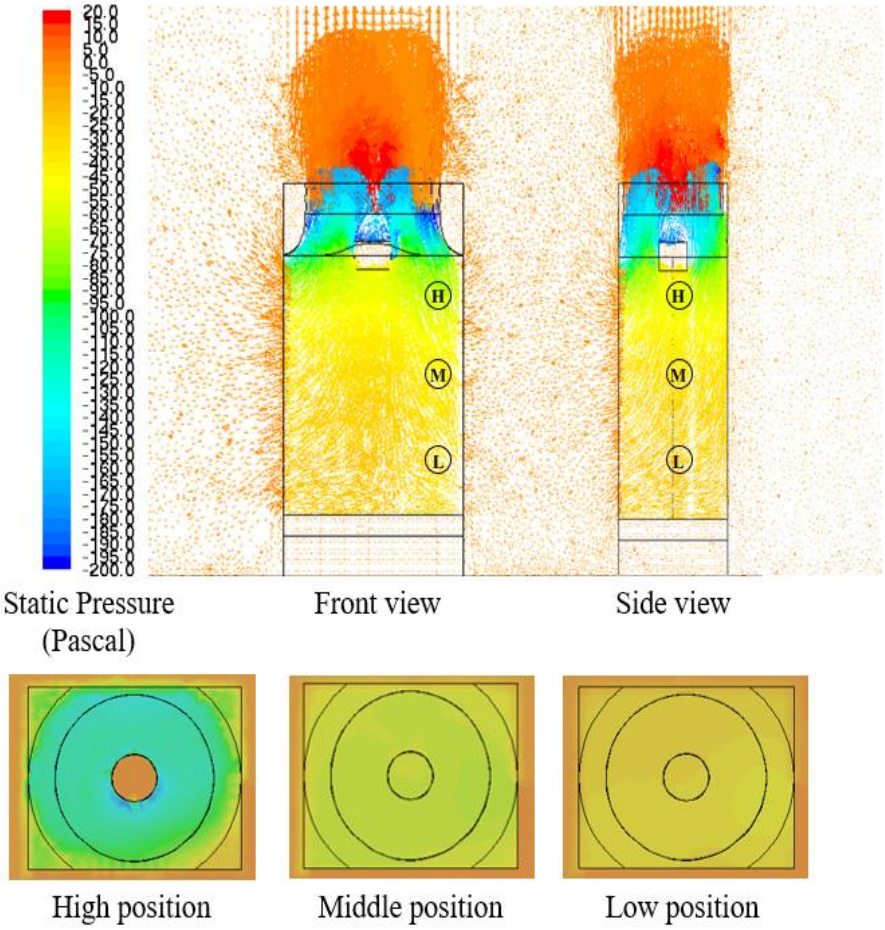

Fig. 3.2 CFD analysis results in no frosting

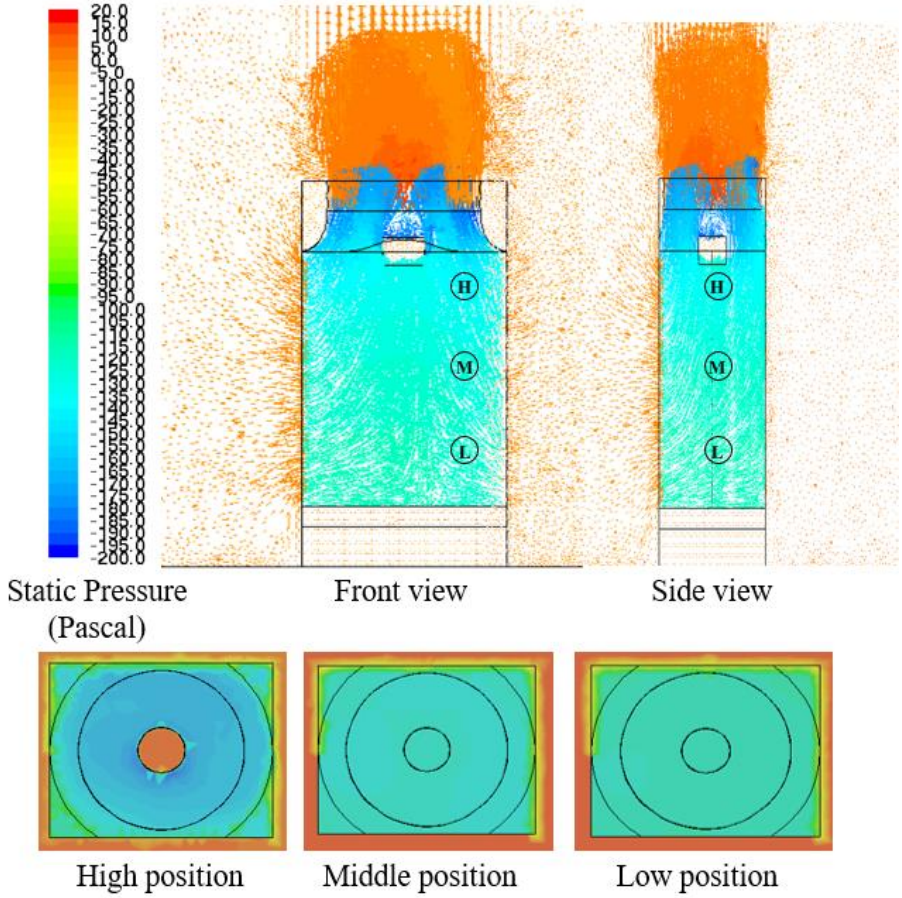

Fig. 3.3 CFD analysis results in frosting

3.4 Summary

The CFD analysis shows that the differential pressure inside of the outdoor unit does not change much at the same height but shows a lot of difference depending on the height.

The pressure values below show differential pressures of high, middle and low under no frosting and frosting conditions. The pressure difference between the no frosting and frosting condition is 45 Pa in a high position and is 80 Pa in a middle position and 95 Pa in a low position.

As the result of this, low position is considered to be optimal position. As the frosting progresses, the progressive state of the frosting can be judged as the pressure value and the accuracy can be increased as the differential pressure value becomes larger.

Chapter 4. Experimental results by measuring differential pressure

4.1 Introduction

The CFD analysis in Chapter 3 shows that the differential pressure inside of the outdoor unit does not change much at the same height but shows a lot of difference depending on the height under frosting and no frosting conditions.

In this chapter, the static differential pressure sensor is established inside of the outdoor unit. Experiment is carried out under several outdoor air conditions and system operation conditions to verify the suggested defrost control method.

Measuring the pressure at the same height, the distance between the measuring point and the heat exchanger is an important factor to consider. The pressure is measured at five locations: center, front, rear, right, and left to find the optimal position at the same height.

The performance of various operating conditions such as pressure measurement position, outdoor air temperature and humidity, and compressor speed is tested to identify the relation of pressure drop with heating capacity of the system. In addition, these experimental results are compared with CFD

analysis results to see how the difference occurs. The pressure difference control method is suggested by providing an appropriate threshold value and the comparing with the result with other estimation methods. According to the experimental results, it is verified that the suggested method can achieve high reliability for the determination of defrost cycle start.

4.2 Optimal position of sensing the static pressure

4.2.1 Optimal position at the same height

Fig. 4.1 shows that pressure differences and heating capacity at the high positon of pressure sensor in Case 1. The result represents that heating capacity decreases because the thermal performance of the heat exchanger degraded as a result of an increase in both the flow resistance and thermal resistance during the frosting. The heating capacity reaches 25 kW maximum in 30 minutes after starting heating operation and the heating capacity decreases to 14kW in 120 minutes after reaching the blocking ratio of 80%. The differential pressure graph at the high position shows that the pressure values according to each measuring position. The left position pressure increases from 112 Pa to 169 Pa, the center position pressure increases from 152 Pa to 190 Pa, the right position pressure increases from 117 Pa to 191 Pa, the front position pressure increases from 139 Pa to 174 Pa and the rear position pressure increases from 100 Pa to 164 Pa. At the beginning of the operation, the pressure is expected to be the highest on the left side close to the fan, but actual measured results show higher pressures measured at the center and front positions. As the frosting progresses, the measured pressure at the center and right positions is the highest. The reason

for this difference is that the shape of the fan blade and the pressure distribution inside the outdoor unit during the frosting.

In order to determine the defrost start time by the differential pressure, the pressure difference between maximum and minimum after operating is important to judge the progress of the frosting. From this point of view, the pressure difference of the right is 59 Pa, the center is 45 Pa, the right is 73 Pa, the front is 50 Pa and the rear is 64 Pa. The right position seems to be optimal at five positions.

Fig. 4.2 shows the differential pressure graph at the middle position. The left position pressure increases from 52 Pa to 150 Pa, the center position pressure increases from 49 Pa to 147 Pa, the right position pressure increases from 41 Pa to 142 Pa, the front position pressure increases from 41 Pa to 139 Pa and the rear position pressure increases from 39 Pa to 138 Pa.

The actual measured results show higher pressures measured at the left and center positions. As the frosting progresses, the measured pressure at the left position is the highest. The pressure difference between maximum and minimum of the right is 98 Pa, the center is 98 Pa, the right is 10 Pa, the front is 98 Pa and the rear is 100 Pa. The right position seems to be optimal at five positions.

Fig. 4.3 shows the differential pressure graph at the low position. The left

position pressure increases from 25 Pa to 129 Pa, the center position pressure increases from 35 Pa to 143 Pa, the right position pressure increases from 27 Pa to 140 Pa, the front position pressure increases from 23 Pa to 132 Pa and the rear position pressure increases from 20 Pa to 132 Pa. The pressure difference between maximum and minimum of the right is 103 Pa, the center is 107 Pa, the right is 112 Pa, the front is 109 Pa and the rear is 112 Pa. The right and rear position seem to be optimal at five positions. The pressure differences between the maximum and minimum measured at the right position near the heat exchanger among the five positions is the highest at the same height.

Therefore, the optimal position of the sensor for measuring the differential pressure is determined as the right position in this study.

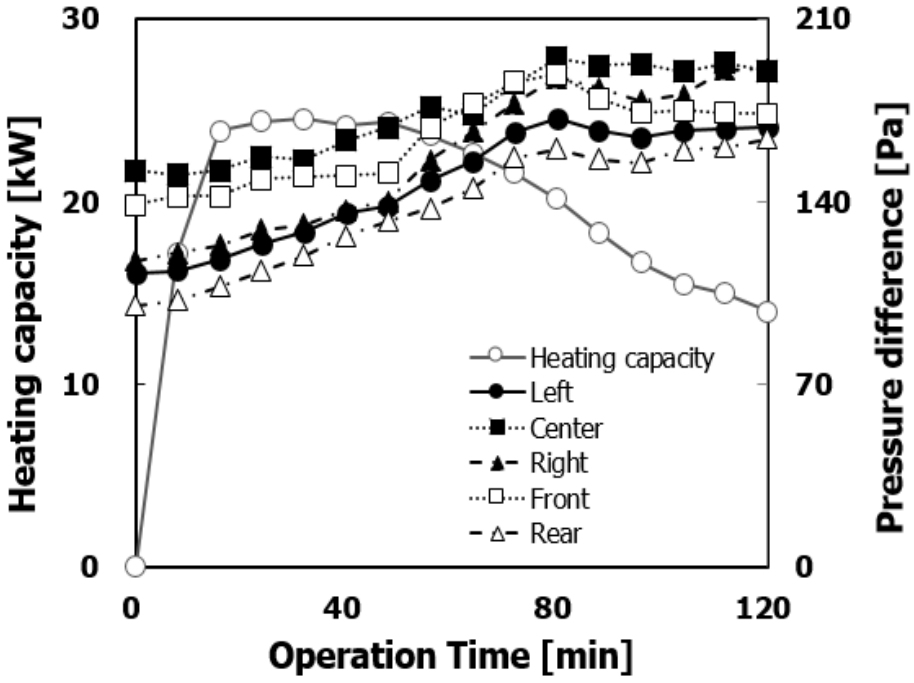

Fig. 4.1 Pressure differences and heating capacity in the high position

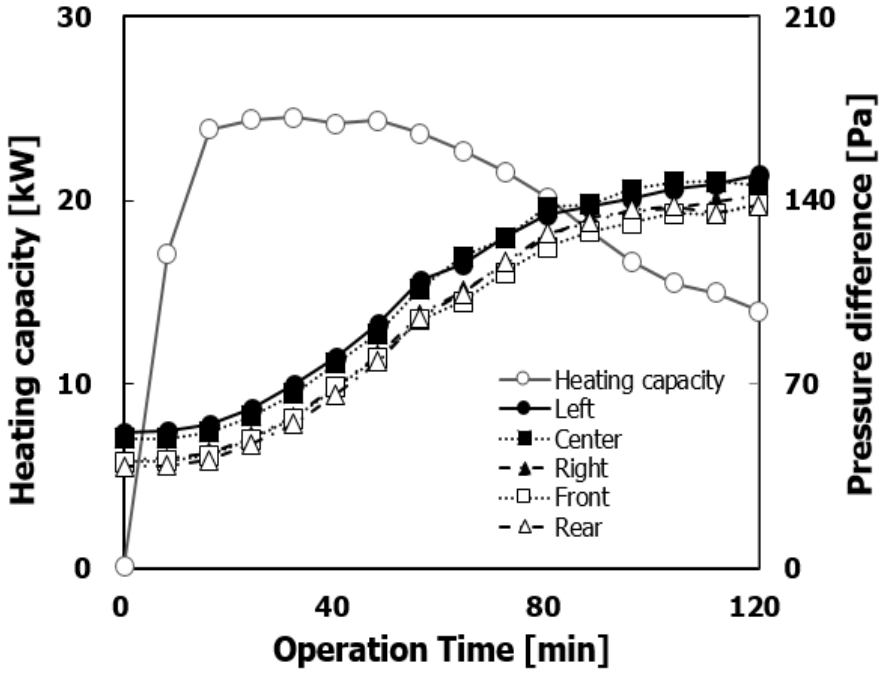

Fig. 4.2 Pressure differences and heating capacity in the middle position

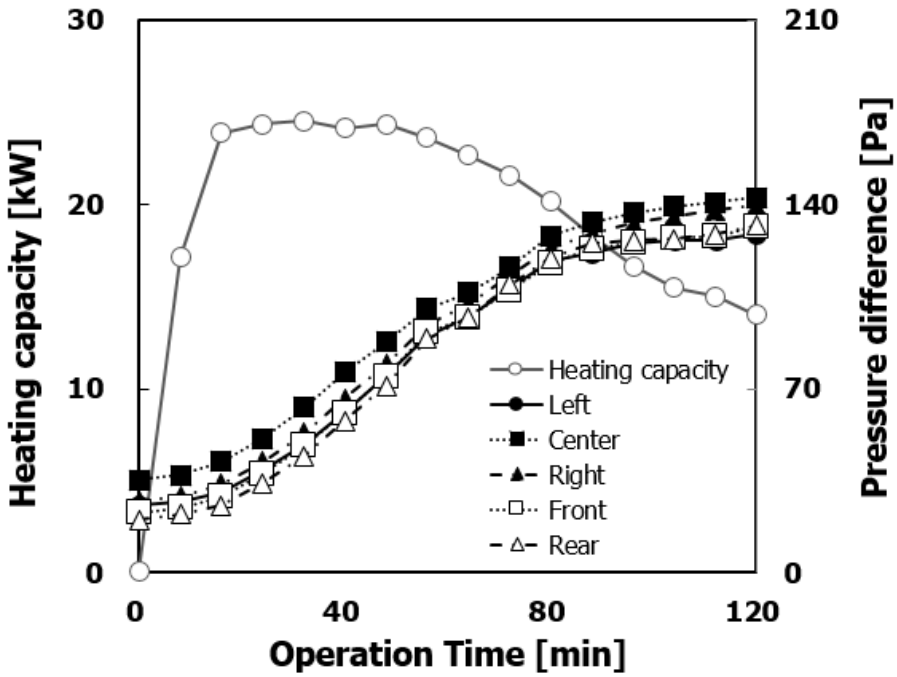

Fig. 4.3 Pressure differences and heating capacity in the low position

4.2.2 Optimal position at the different height

Fig. 4.4 shows the pressure changes are measured at high, middle, and low positions based on the optimal pressure measurement position at the same height in the previous experiment. The differential pressure graphs represent that the pressure of the high position increases from 117 Pa to 191 Pa, the pressure of the middle position increases from 41 Pa to 142 Pa, and the pressure of the low positon increases from 27 Pa to 140 Pa.

In order to determine the defrost start time by the differential pressure, the pressure difference between maximum and minimum after operating is important to judge the progress of the frosting. From this point of view, the pressure difference of high is 73 Pa, the middle is 101 Pa, the low is 112 Pa. The reason for the lowest initial pressure value measured at the low position is the farthest away from the fan. The initial pressure difference between high and low was 90 Pa after starting and it decreased to 50 Pa during the frosting.

As the frosting progresses, the pressure inside the outdoor unit becomes a little bit balanced and the pressure decrease value according to the distance to the fan becomes smaller.

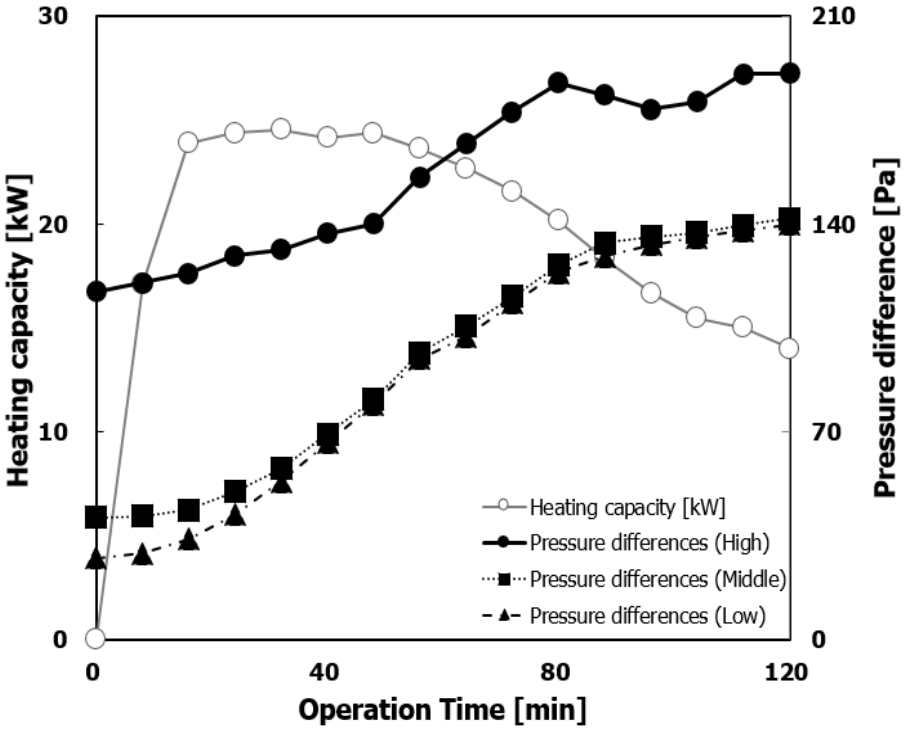

Fig. 4.4 Pressure differences and heating capacity according to measuring position

The position of low seems to be optimal at three positions. In previous experiments, the right close to the heat exchanger and low position is considered to be optimal position and the additional experiments are conducted under various conditions in Table 2.3.

4.3 Pressure differences under various conditions

4.3.1 Various dry-bulb temperature conditions

Fig. 4.5 shows that heating capacity ratio and pressure difference variation for different dry bulb temperature conditions are listed in Table 2.3. While heating capacity of Case. 3 is the highest due to the high outdoor air temperature, performance drop rate is similar regardless of the outdoor temperature because relative humidity of the conditions are same. Pressure drop of Case. 2 is higher than Case. 1 and Case. 3 contrary to heating capacity. It is because the low outdoor air temperature accelerates frosting and it increases the air resistance of the conditions are same. Pressure drop of Case. 2 is higher than Case. 1 and Case. 3 contrary to heating capacity. It is because the low outdoor air temperature accelerates frosting and it increases the air resistance of the heat exchanger. Relative heating capacity ratio means that when it reaches 80% of its maximum value. When relative heating ratio is 0.8 and the pressure

difference is over 126 Pa, it is proper time to start the defrosting cycle. From this point of view, Case. 1, Case. 2 and Case 3 show that the intersection of the performance ratio with 0.8 is near 126 Pa.

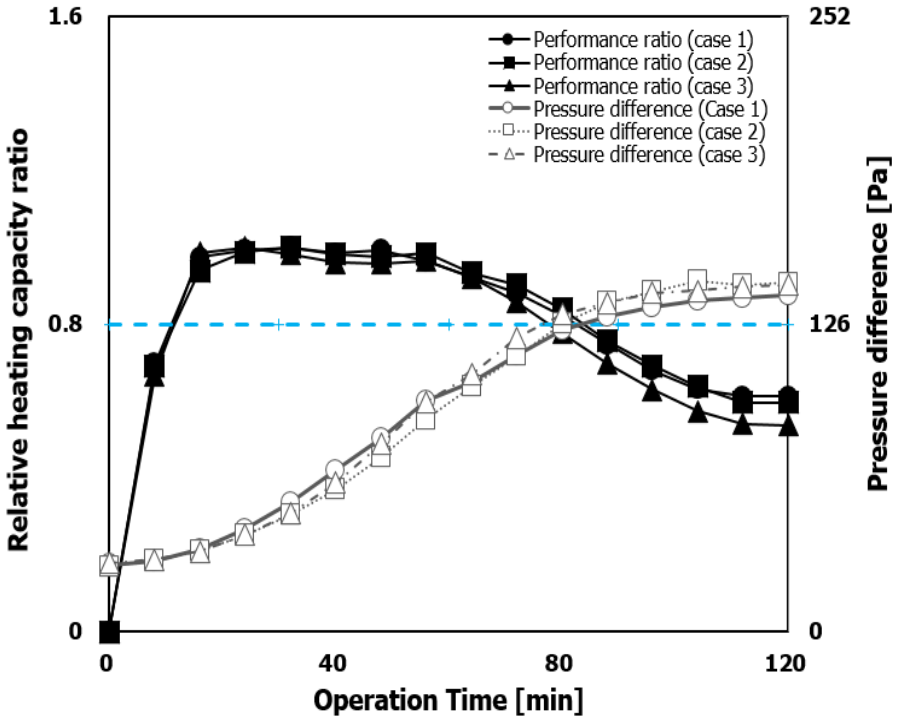

Fig. 4.5 Heating capacity ratio and pressure differences under various dry-bulb temperature

4.3.2 Various relative humidity conditions

Heating capacity ratio and pressure differences for different relative humidity conditions are shown in Fig. 4.6. Even though the frosting rate is different according to the humidity conditions, heating performance drop rate is similar to the increase rate of pressure differences. At the same temperature condition, the higher the relative humidity, the faster the frosting occurred. Therefore, the Case. 5 which has the highest relative humidity, shows the fastest rate of decrease of heating capacity and the rate of increase of differential pressure. The relative heating capacity ratio is near 0.85 when pressure difference is 126 Pa.

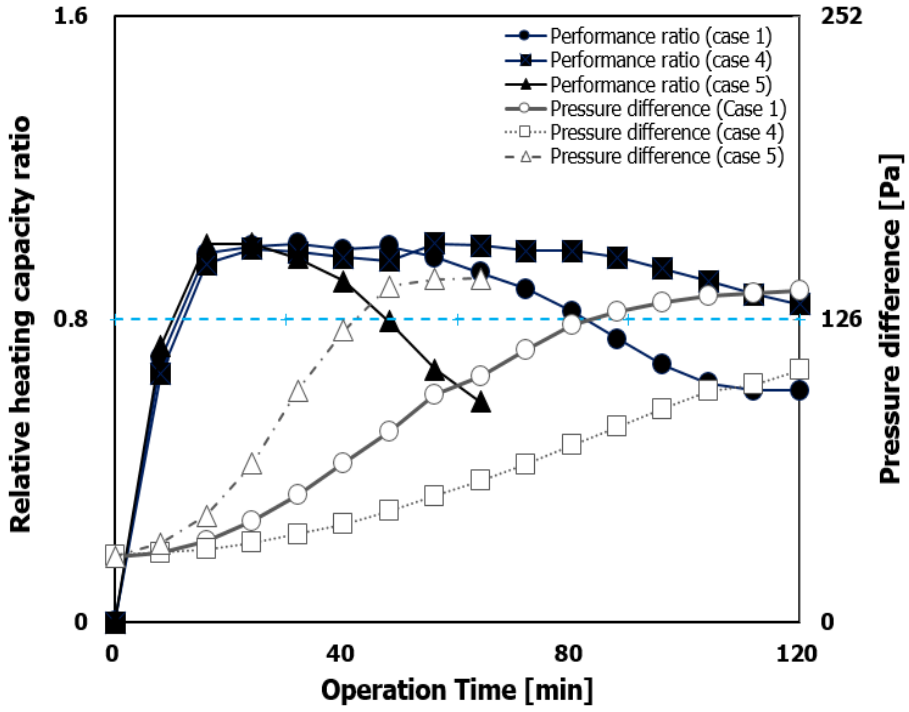

Fig. 4.6 Heating capacity ratio and pressure differences under various relative humidity

4.3.3 Various compressor speed conditions

Fig. 4.7 shows heating capacity and pressure differences under different compressor speed conditions.

The heating capacity in Case. 6 which is 25% lower than the standard compressor speed is about 19 kW (78% of 25 kW) after stabilizing the heating cycle. In Case. 6, the frosting progresses slowly due to the low speed of the compressor. However, the pressure differences are similar to Case. 1 in 100 minutes.

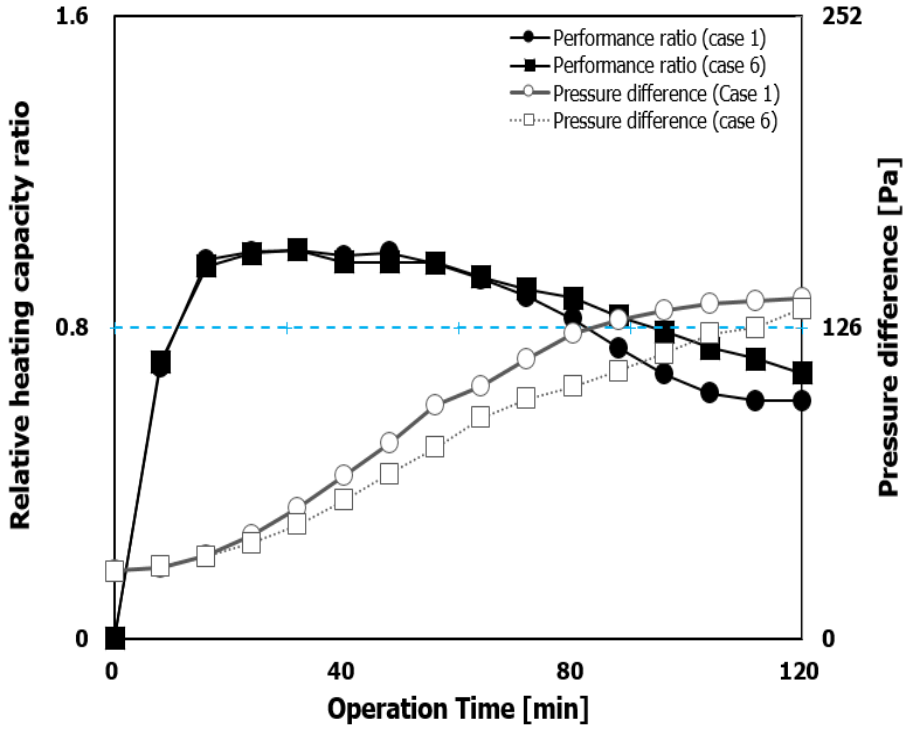

Fig. 4.7 Heating capacity ratio and pressure differences under various compressor speed

4.3.4 Various fan speed conditions

Fig. 4.8 shows heating capacity and pressure differences under different fan speed conditions. The differential pressure of Case. 7 which is 20% higher than the standard fan speed, increases 50% compared to Case. 1, up to 211 Pa. Case. 8 which has a fan speed of 20% lower than standard, has maximum 94 Pa of differential pressure. It is 32% lower than Case. 1. Therefore, it can be seen that the differential pressure value with during the frosting increases in proportion to the fan speed.

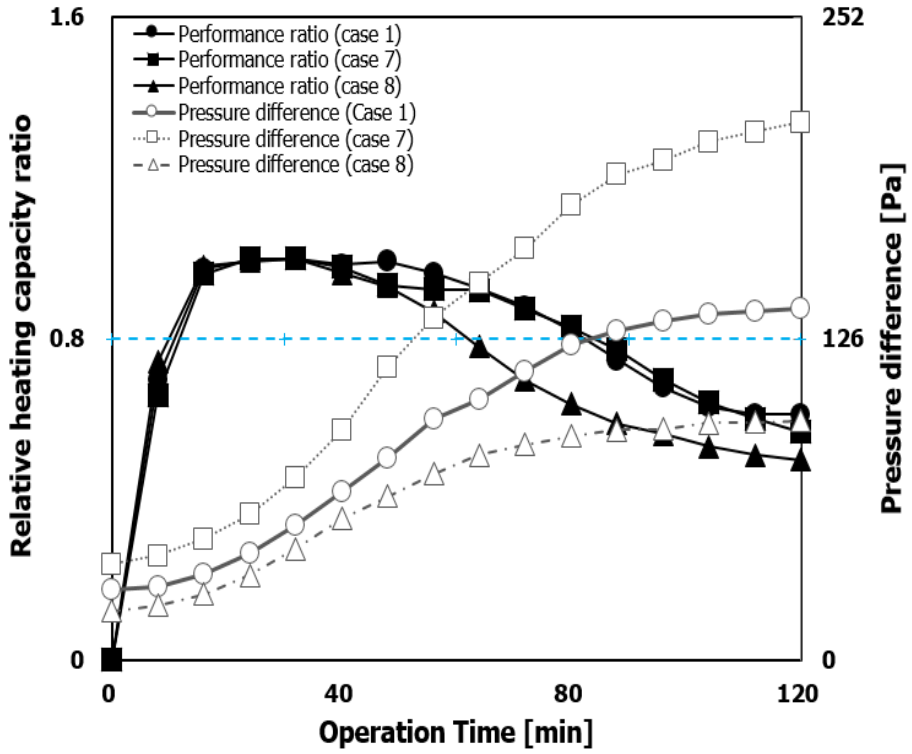

Fig. 4.8 Heating capacity ratio and pressure differences under various fan speed

4.4 Summary

The determination method based on the pressure difference is suggested, proper defrosting cycle start should be defined, Jhee et al. (2002) reported that defrost cycle be started when frost blocks 70~80 % of frontal area of heat exchanger. Kim et al. (2015) establish the criteria that proper defrosting cycle start time is set to the time when heating capacity decreased to 50 % of its maximum value. In this paper, it is set to the time when heating capacity reaches 80 % of its maximum value as expressed in Eq. (4.1)

$$\dot{Q}_{t=t_{std}} = 0.8\dot{Q}_{max} \tag{4.1}$$

To determine the thresholds of the pressure difference control method, each value of pressure difference at the proper defrost cycle start time is averaged for all the experimental conditions. As a result, 126 Pa is set to the thresholds. Similar procedure is done to set the thresholds of time control method.

The thresholds for time control is set to 81 min. Relative errors of different pressure control and time control for the proper defrost time is listed in Table 4.1. While the error still remains for the pressure difference control, it is much

improved compared to the time method. Average error is 4.4 % for the pressure difference control method. Average error is 21.1 % for the conventional time control method. The pressure difference control method denotes 16.7 % point improvement than the conventional time control method. Especially, when the fan speed is constant, the average error in Case. 1 ~ 6 is 1.0 %, which is 3.3 % higher than the 4.3 % of the conventional time control method.

However, Case. 7 and 8 where the fan speed is changed, the average error is quite high as 14.4 %. The reason is that changes of the fan speed can change the performance curve of the fan affecting airflow and static pressure.

Table 4.1 Comparison of the defrost cycle start time according to the different determination method

Case number	T_{std}[min]	Error of T_{tdc} (%)	Error of T_{tc} (%)
Case 1	82	-0.2	-1.2
Case 2	83	-1.2	-2.4
Case 3	78	-1.3	3.8
Case 4	120	4.8	-34.7
Case 5	46	-8.7	76.1
Case 6	94	12.8	-13.8
Case 7	86	-17.4	-5.8
Case 8	62	-11.3	30.6

Chapter 5. Conclusion

Determination technique of defrost cycle start time based on the static pressure difference sensor is suggested. The CFD analysis shows that the differential pressure inside of the outdoor unit does not change much at the same height but shows a lot of difference depending on the height. It shows that the low position of measuring the static pressure is considered to be the optimal position.

Experiment of the heat pump operation under frosting condition is carried out under various conditions to verify the reliability of the pressure difference control method. As a result, the determination time based on the suggested method is more accurate about 21.1% points compared to the conventional time control method.

References

Wang, W., Xiao, J., Guo, QC., Lu, WP., Feng, YC., 2011. Field test investigation of the characteristics for the air source heat pump under two typical mal-defrost phenomena, Applied Energy12(88), 4470-80

Breque, F., Nemer, M., 2017, Modeling of a fan-supplied flat-tube heat exchanger exposed to non-uniform forst growth, International Journal of Refrigeration 75, 129-140

Song, M.G., Deng, Shimingb., Dang, Chaobina., Mao, Ningc., Wang, Zhihuad., 2018, Review on improvement for air source heat pump units during frosting and defrosting, Applied Energy 211, 1150-1170.

Zhu, J.H., Sun, Y.Y., Wang, W., Deng, S.M., Ge, Y.J. and Li, L.T., 2015, Developing a new frosting map to guide defrosting control for air-source heat pump units, Applied Thermal Engineering 90, 782-791.

Kim, M.H., Lee, K.S., 2015, Determination method of defrosting start-time based on temperature measurements, Applied Energy 146, 263-269.

Jiang, Y., Dong, J., Qu, M., Deng, S., Yao, Y., 2013, A novel defrosting control method based on the degree of refrigerant superheat for air sourece heat pumps, International Journal of Refrigeration 36, 213-22

Mengjie, S., Shiming, D., Chaobin, D., Ning M., Zhihua, W., 2018, Review on improvement for air source heat pump units during frosting and defrosting, Applied Energy 211, 1150-1170

Zhu, J.H., Sun, Y.Y., Wang, W., Deng, S.M., Ge, Y.J. and Li, L.T., 2015, Developing a new frosting map to guide defrosting control for air-source heat pump units, Applied Thermal Engineering 90, 782-791.

Ge, Y., Sun, Y., Wang, Y., Wang, W., Zhu, H., Li, L., Liu, J., 2016, Field test study of a novel defrosting control method for air-source heat pumps by applying tube encircled photoelectric sensors, International Journal of Refrigeration 66, 133-144.

Byun, J.S., Jeon, C.D., Jung, J.H. and Lee, J., 2006, The application of photo-coupler for frost detecting in an air-source heat pump, International Journal of Refrigeration 29, pp.191-198.

Wang, W., Xiao, J., Feng, Y., Guo, Q. and Wang, L., 2013, Characteristics of an air source heat pump with novel photoelectric sensors during periodic frost–defrost cycles, Applied Thermal Engineering 50, 177-186.

Kim, M.H. and Lee, K.S., 2015, Determination method of defrosting start-time based on temperature measurements, Applied Energy 146, 263-269.

Shao, L., Riffat, S.B., 1995, Accuracy of CFD for Predicting Pressure Losses in HVAC Duct Fittings, Applied Energy 51, 233-248.

Carstens, M., Xia, Z., Yadavalli, S., 2018, Measurement uncertainty in energy monitoring : Present state of the art, Renewable and Sustainable Ennergy Reviews 82, 2791-2805

Varun, Singh., Omar, Abdelaziz., Vikrant, Aute., Reinhard, Radermacher., 2011, Simulation of air-to-refrigerant fin-and-tube heat exchanger with CFD-based air propagation, International Journal of Refrigeration 34, 1883-1897.

Jhee, S., Lee, K.S, Kim, W.S., 2002, Effect of surface treatments on the frosmting/defrosting behavior of a fin-tube heat exchanger, International Journal of Refrigeration 25,1047-53

국 문 초 록

본 연구에서는 공기열원 열펌프 시스템에서 착상에 따라 발생되는 실외기 내부의 압력과 실외기 외부의 대기압과의 압력 차이를 측정하여 최적의 제상 시작 시간을 결정하기 위한 검출 방법을 제안하고 CFD 해석 및 실험을 통해 검증하였다. 일반적으로 착상은 공기 온도가 낮고 습도가 높은 환경에서 열교환기의 표면온도가 주변의 공기의 이슬점 온도보다 낮을 때 발생한다. 착상이 진행함에 따라 열교환기 표면에 서리 축적이 증가하며 이 영향으로 실외기 내부와 외부의 공기 압력 차이가 발생한다. 이러한 압력 변화의 차이를 측정하여 착상 진행의 정도를 예측할 수 있었다. 공기의 압력은 정압과 동압으로 구성되며 정압은 공기 유동에 대해 일정하고 신뢰할 수 있는 데이터를 얻을 수 있다. 동압은 공기의 유속과 방향에 영향을 많이 받게 되며 또한, 먼지 및 습기 등에 의해 압력 측정 장치의 신뢰성을 저하시킬 수 있다. 실외기 팬이 동작하면 실외기 내부의 압력이 외부의 대기압보다 낮아져 부압이 발생하게 되며 정압을 이용하게 되면 센서 내부의 먼지나 습기의 영향을 최소화 할 수 있다. 실외기 내부의 압력 측정 위치 선정은 이 연구에서 중요한 요소이며 CFD 해석과 사전 실험을 최적의 위치를 찾고 실외 공기 온도, 실외 공기 습도, 압축기 속도, 실외 팬 속도와 같은 다양한 조건에서 실험을 진행하였다. CFD 해석을 통해 실외기 내부와 외부의 차압은 측정 위치의 높이에 따라 많은 차이가 발생하는 것을 알게 되었고 실험을 통해서는 최적의 차압 측정 위치를 선정 할 수 있었다.

CFD해석 및 사전 실험의 결과로 선정된 압력 차이가 가장 많이 발생하는 최적의 위치에 압력센서를 설치하고 다양한 실험조건에서 측정된 차압의 변화를 통해 제상 시작 시간을 예측하고 기존의 시간 제어 방법과 비교한 결과 약 21.1% 정확도가 개선되었다. 이 연구는 공기열원 열펌프 시스템에서 최적의 제상 시작 시간 판단을 위해 유용하게 쓰일 수 있다.

주요어: 공기열원 열펌프, 착상, 제상, 차압
학번: 2016-27922